ELSEVIER

Aerosol Science 35 (2004) 1–19

Journal of
Aerosol Science

www.elsevier.com/locate/jaerosci

Improved numerical simulation of aerosol deposition in an idealized mouth–throat

E.A. Matida, W.H. Finlay*, C.F. Lange, B. Grgic

Department of Mechanical Engineering, University of Alberta, Edmonton, Alberta, Canada, T6G 2G8

Received 14 June 2002; received in revised form 11 November 2002; accepted 11 November 2002

Abstract

The deposition of monodisperse particles (1.0–26.0 μm diameter) in an idealized mouth–throat geometry has been studied numerically. The continuous phase flow is solved using a RANS (Reynolds averaged Navier–Stokes) turbulence model at inhalation flow rates of 90.0 and 30.0 l/min. The particulate phase is simulated using a random-walk/Lagrangian stochastic eddy-interaction model (EIM). Without near-wall corrections in the EIM, poor agreement is seen with experimental data on deposition. However, when a new near-wall correction in the EIM is implemented, the particle deposition results in the idealized mouth–throat geometry are in relatively good agreement when compared with measured data obtained in separate experiments.

1. Introduction

Medication in the form of solid (dry-powder) or liquid particles (droplets) is commonly inhaled by human patients in the treatment of lung diseases. Due to the filtering characteristics of the nasal tract, the aerosol is generally inhaled through the oral cavity, and then passes the pharynx, the larynx and the trachea before reaching the lung. Although the lung is the final target, part of the dose will deposit on the walls of the mouth–throat (extrathoracic) region, giving losses and departure from the ideal delivery. This can result in a less efficient and more costly treatment in addition to unwanted side effects. As a result, deposition in the mouth–throat region itself becomes an important issue. This deposition depends on a number of factors (Finlay, 2001) including the airway geometry of the patient, the inhaled mass flow rate, the characteristics of the particles (diameter distribution, density, shape, hygroscopicity, etc.), as well as pharmaceutical inhalation device (DeHaan & Finlay, 2001). Experimental deposition studies, summarized by Stahlhofen, Rudolf, and James (1989) in human

* Corresponding author. Tel.: +1-780-492-4707; fax.: +1-780-492-2200.
E-mail address: warren.finlay@ualberta.ca (W.H. Finlay).

0021-8502/$ - see front matter © 2003 Elsevier Ltd. All rights reserved.
doi:10.1016/S0021-8502(03)00381-1

Nomenclature

C_μ	coefficient in the k–ε turbulence model
d	mass median diameter, m
f	function
g	gravitational acceleration, m/s^2
k	turbulence kinetic energy, m^2/s^2
L_e	length scale of fluid eddy, m
N, n	number
Q	mass flow rate, l/min
Re_p	particle Reynolds number ($=U_r d_p/\nu_f$)
r, s, t	Local coordinate system
t	time, s
U_r	relative velocity, m/s
u^*	friction velocity, m/s
u_e	velocity scale of fluid eddy, m/s
u, v, w	axial, radial and azimuthal velocities, m/s
x, y, z	Cartesian coordinate system directions
y^+	dimensionless distance from the wall, m

Greek letters

α	coefficient for Reynolds number effect on viscous drag, s
β	ratio of Lagrangian time scale to Eulerian time scale
ε	dissipation rate of turbulence kinetic energy, m^2/s^3
ϕ	variables
λ	Taylor microscale, m
μ	dynamic viscosity, N s/m^2
ν	kinematic viscosity, m^2/s
ρ	density, kg/m^3
τ_e	lifetime of fluid eddy, s
τ_p	relaxation time of particle, s
τ_p^+	dimensionless relaxation time of particle ($=d_p^2\rho_f^2 u^{*2}\rho_p/18\rho_f\nu_f^2$)

Subscripts

e	eddy
dep	deposition
f	fluid
i	index
L	Lagrangian
p	particle
rms	root-mean-square (RMS) value

Superscripts

$(^-)$	average
$(\ )'$	fluctuation
$(\ )^+$	non-dimensionalization by wall variables (u^* and ν_f)

subjects, as well as computational analysis (Stapleton, Guentsch, Hoskinson, & Finlay, 2000; Sarangapani & Wexler, 2000 using the nasal tract; Yu, Zhang, & Lessman, 1998 for particle diffusion in human upper respiratory system and Li et al., 1996 for deaggregation of particles) have appeared in the literature, but deposition of particles in the mouth–throat region remains poorly understood.

To gain a better understanding of mouth–throat deposition, numerical simulation is useful. Numerical studies predicting the rate of deposition of particles onto the walls of turbulent flows are usually handled by Eulerian or Lagrangian approaches. Various drawbacks present in the Lagrangian and Eulerian models were reviewed by Elgobashi (1994). In an Eulerian approach, particles are assumed to move towards the wall by turbulent diffusion, and then reach the wall by a free flight mechanism. Friedlander and Johnstone (1957), Beal (1970), Ganic and Mastanaiah (1981), Lee and Wiesler (1987), Yang and Lee (1991) used an Eulerian approach to simulate the deposition of particle in turbulent pipe flows. Young and Leeming (1997) studied the deposition problem (again in turbulent pipe flows) using a two fluid Eulerian approach, where the particulate phase is considered as a continuum having conservation equations of mass and momentum in an Eulerian coordinate system similar to those of the fluid. These equations were Reynolds averaged, leading to a number of turbulence equations, two of them being particularly important: one representing the 'turbulent diffusion' and the other the 'turbophoresis' (Reeks, 1983). In the literature survey performed by the present authors, it seems that these Eulerian approaches have not been extended to more complex geometries such as the mouth–throat deposition problem.

As noted by Young and Leeming (1997), the Eulerian free-flight model is a consistent physical model and the calculation is very fast, but it does not totally explain how particles acquire a velocity towards the wall nearly equal to the friction velocity u^* at a stopping distance from the wall between $1 < y^+ < 10$, a region where the RMS velocities of the primary flow are much less than u^*. The two fluid Eulerian model is based on rigorous analysis, but still presents some difficulties related to the modeling of the time-averaged momentum equation (Elgobashi, 1994).

In a Lagrangian approach, the primary flow is calculated by using DNS (direct numerical simulation), LES (large Eddy simulation) or RANS (Reynolds averaged Navier–Stokes) equations (for example, the k–ε or k–ω turbulence model equations). Then, individual particles are numerically released in the calculated flow, and move according to the particle equation of motion. When the particle concentration is very low, the primary flow is assumed to be unmodified by the presence of particles (i.e., one-way coupling), an assumption that significantly facilitates the simulation of the motion of particles. On the other hand, when the particle concentration is not low, the mutual interaction between the primary flow and the particles must be incorporated into the simulation (i.e., two-way coupling). Chen and McLaughlin (1995), Uijttewaal and Oliemans (1996) and Wang, Squires, Cheng, and McLaughlin (1997) used large eddy simulation (LES) and direct numerical simulation (DNS) to study particle motions in turbulent channel or pipe flows. In the analysis of the motion of particles, RANS models are normally used together with eddy interaction models (EIM, or random walk models), a Lagrangian stochastic approach where individual particles are allowed to interact successively with discrete eddies, each eddy having length, velocity and lifetime characteristic scales obtained from the primary flow calculation results.

DNS is the most accurate way to simulate turbulent flow and to study dispersed systems. However, DNS demands long computing times and large memory capacities, restricting the applicability of DNS when studying the motion of particles in boundary layer flow to low Reynolds numbers and

short simulation times. LES permits calculation at higher Reynolds numbers, but at the same time valuable information concerning the small scales structures are lost, and may affect the Lagrangian calculation of very small particles. In addition, LES has also a relatively high computing cost and better closure models are necessary in order to employ LES in the two-way coupling regime (see again Elgobashi, 1994).

Due to its relative simplicity, it seems that RANS/EIM is preferred in engineering applications. EIM itself has its limitations, namely: (1) Particles with size comparable to an eddy cannot be accurately treated, (2) The motion of a particle does not take into account the effect of neighboring particles, (3) Two-way coupling effects are not considered, (4) EIM does not preserve the divergence properties of the imposed mean flow (see MacInnes & Bracco, 1992), i.e., tracer particles calculated using EIM tend to be concentrated where the turbulence intensity is low and drift away from regions of higher turbulence intensities. The method of sampling the velocity when using an EIM leads to this "spurious drift" velocity.

Despite such drawbacks, EIM is still an attractive tool to be used within the framework of the widely used RANS turbulence models as pointed out by Wang and James (1999), who proposed damping functions to reconstruct the fluctuating part of the flow field. EIM is specially suitable for a complex geometry such as the mouth–throat, where the cost of computation is a concern. Stapleton et al. (2000) previously applied EIM and RANS to model turbulent aerosol deposition in the mouth–throat. They showed, however, that the classical EIM (Gosman & Ioannides, 1981) allied with the k–ε turbulence model grossly overestimated deposition for the lower values of the inertial parameter, $\rho_p d_p^2 Q$. In the present work, the EIM and RANS turbulence modeling for the turbulent aerosol deposition in the mouth–throat region is thoroughly investigated and a new near-wall correction in the EIM to circumvent overestimation of total deposition is proposed.

2. The mouth–throat geometry

An idealized mouth–throat model geometry developed at ARLA (Aerosol Research Laboratory of Alberta) (Stapleton et al., 2000; DeHaan & Finlay, 2001; Grgic, Finlay, & Heenan, 2002) is adopted here (see Fig. 1). This geometry is an average geometrical model for adults based on information available in the literature, supplemented with separate measurements using computed tomography (CT) scans of patients ($n = 10$) with no visible airway abnormalities and by the observation of living subjects ($n = 5$). The trachea is modeled as a smooth vertical cylinder having 62.0 mm of length and 16.0 mm of diameter. The larynx is an elliptical tube with a glottal opening with major axis of 12.0 mm and minor axis of 10.0 mm. The epiglottal folds are protruded inside the pharynx and form a tube that joins the glottis. The epiglottis is approximately 20.0 mm above the base of the pharynx. The pharynx is an elliptical cylinder with anterior and posterior walls nearly parallel. The bottom ellipse of the pharynx has a major axis of 30.0 mm and a minor axis of 12.2 mm. The top ellipse of the pharynx has a major axis of 23.8 mm with the same 12.2 mm of minor axis. The pharynx length is 41.9 mm. The vault of the mouth in a coronal section is a segment of a circle whose radius decreases approaching the mouth opening (simplified as a circle of 23.6 mm). A cylindrical mouthpiece of 17.0 mm in diameter and 119.0 mm in length is used. The bottom part of the oral cavity is joined smoothly with the pharynx. The upper walls of the oral cavity join the middle plane of the top ellipse of the pharynx.

Fig. 1. Mouth–throat idealized geometry.

Experiments on the deposition of aerosols in casts of this mouth–throat geometry indicate that our idealized mouth–throat geometry duplicates average filtering efficiencies in vivo (DeHaan & Finlay, 2001; Rahmatalla, Zuberbuhler, Lange, & Finlay, 2002). Further demonstration of this is given in Fig. 2 where deposition in casts of our idealized airway geometry was obtained by Grgic et al. (2002) for two flow rates ($Q = 30.0$ and 90.0 l/min) and compared to the in vivo curve fits of Stahlhofen et al. (1989). The maximum and minimum (95% confidence interval) of Stahlhofen et al.'s (1989) in vivo data are also shown in Fig. 2.

3. Primary flow solution

The governing equations of fluid motion (Navier–Stokes equations) were solved numerically in the above described idealized mouth–throat geometry with an entry pipe region and using CFX-Tascflow (version 2.11, AEA Technology Engineering Software, Ltd.) An IGES (Initial Graphics Exchange Specification) mouth–throat geometry file from Grgic et al. (2002) was imported using CFX-Build (AEA Technology Engineering Software, Ltd.). A structured grid having 125 blocks was created from this file. The grid contains approximately 1,050,000 hexahedric elements, with biased accumulation of nodes towards the wall. See Fig. 3 for a view of the grid at the middle plane section of the geometry. The importance of grid resolution on particle deposition is discussed in Section 7. Following the study by Stapleton et al. (2000), a standard k–ε turbulence model was first tested for comparison reasons and the results are shown in Section 8. Then, a modified linear profile scheme that gives second order error reduction in most instances was used in the discretization of the equations and the fluid flow was solved using the standard k–ω turbulence model (Wilcox, 1988) with Kato and Launder

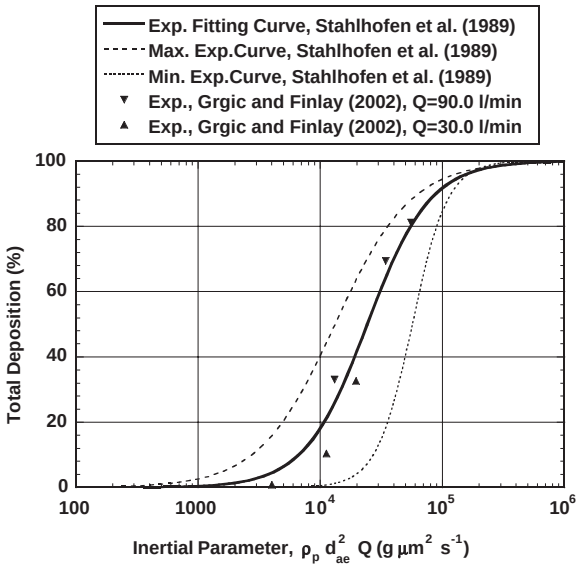

Fig. 2. Total deposition (or deposition efficiencies—mass fraction between the aerosol deposited onto the mouth–throat region and the total inhaled aerosol) for different sets of experiments: Stahlhofen et al. (1989) in human subjects and Grgic et al. (2002) in an idealized mouth–throat cast.

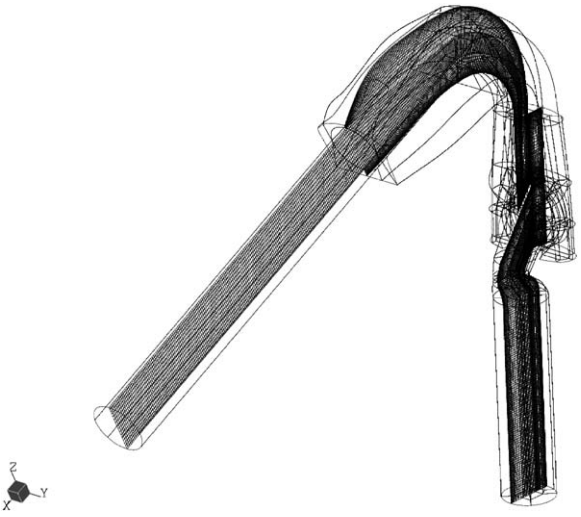

Fig. 3. Middle-plane mesh of an idealized mouth–throat geometry.

modification (Kato & Launder, 1993) (see also documentation of CFX-TASCflow Version 2.11 software, AEA Technology Engineering Software, Ltd.). For the inlet conditions, a fully developed mean pipe flow velocity profile for flow rates of 90.0 and 30 l/min, a turbulence intensity of 5% of the mean velocity and a turbulence length scale of 10% of the inlet diameter are used.

4. Eddy Interaction Model (EIM)

An Eddy interaction model (EIM) (see Graham & James, 1996; Wang & Stock, 1992, for details) is a Lagrangian method of simulation used to numerically track liquid or solid particles released in turbulent flows. Some authors (MacInnes & Bracco, 1992) have used the term 'random walk' to describe this type of model, where one particle is allowed to interact successively with various eddies. Each eddy has a characteristic lifetime, length and velocity scales. The end of interaction between the particle and one eddy occurs when the lifetime of the eddy is over or when the particle crosses the eddy. At this instant, a new interaction with the particle and a new eddy is started. The trajectory of this particular particle is obtained by solving the particle equation of motion (see for example, Kim, Elgobashi, & Sirignano, 1998; Mei, 1996 or Maxey & Riley, 1983). In order to obtain velocity or deposition statistics, hundreds of particles must be released into the flow. On the basis of the method of Gosman and Ioannides (1981), Schuen, Chen, and Faeth (1983) simulated the particle dispersion in a turbulent round jet, where they used a k–ε turbulence model along with the following characteristic scales of fluid eddies:

$$L_e = (C_\mu)^{3/4} \frac{k^{3/2}}{\varepsilon}, \tag{1}$$

$$\tau_e = \frac{L_e}{(2k/3)^{0.5}} \tag{2}$$

and

$$u_e = \sqrt{\frac{2}{3}\, k}. \tag{3}$$

Kallio and Reeks (1989) derived an empirical equation for the eddy lifetime near the wall ($y^+ < 200$) of a turbulent pipe. In order to give self-consistent dispersion properties, the eddy lifetime was specified by randomizing the lifetime scale from an exponential probability density function. Following the work of Wang and Stock (1992), Graham and James (1996) pointed out that in the case when lifetime scales τ_e are specified to be constant in time, the choice of $\tau_e = 2\tau_L$ ensures dispersion consistency. Here τ_L is the Lagrangian fluid time scale. Schuen et al. (1983) used the case $\tau_e = 2\tau_L$. Graham and James (1996) also concluded that to reduce computational costs, the constant eddy lifetime scheme is preferred over an exponentially decaying lifetime scheme.

The Lagrangian time scales are a function of the Eulerian time scale $\tau_L = \beta\tau_E$. Here, β is a function of the turbulent Reynolds number ($Re_\lambda = u'\lambda/\nu$), varying from 0.6 to 0.3 for $Re_\lambda = 20$ to 70, according to Sato and Yamamoto's (1987) measurements. Hinze (1975, p. 426) has proposed $\beta \cong 0.4$. According to Hinze (1975), the Lagrangian time scale is the largest interval in time that a Lagrangian particle will continue moving in that direction. It must be pointed out that there is some controversy over the correct value that $\tau_L/(k/\varepsilon)$ must take (MacInnes & Bracco, 1992). Here we use Schuen's model as given in Eqs. (1)–(3).

Much more complex models than Schuen's model, for example Hennick and Lightstone (2000), Burry and Bergeles (1993), Zhou and Leschziner (1991) or Berlemont, Desjonqueres, and Gousbet (1990) have appeared in the literature, but they are beyond the scope of the present study and their assessment will be postponed for future work.

5. Particle equation of motion

Considering relatively small particles with low density ratios $\rho_f/\rho_p \ll 1$ and taking into account only viscous drag and gravity, the following three-dimensional Lagrangian equations that describe the movement of a particle in the Cartesian coordinate system are adopted in the present simulation (for details, see Kim, Elgobashi, & Sirignano, 1998; Mei, 1996; Maxey & Riley, 1983):

$$\frac{du_p}{dt} = \frac{(u_j - u_p)}{\tau_p/\alpha}, \tag{4}$$

$$\frac{dv_p}{dt} = \frac{(v_j - v_p)}{\tau_p/\alpha}, \tag{5}$$

$$\frac{dw_p}{dt} = \frac{(w_f - w_p)}{\tau_p/\alpha} - g\left(1 - \frac{\rho_f}{\rho_p}\right), \tag{6}$$

where the particle relaxation time is

$$\tau_p = \frac{\rho_p d_p^2}{18\mu_f} \tag{7}$$

and

$$\alpha = 1 + 0.15Re_p^{0.687} \tag{8}$$

Here Re_p is the particle Reynolds number. Note that the fluid velocity components in Eqs. (4)–(6) are instantaneous quantities composed of the mean part and the fluctuating part; for example

$$u_f = \bar{u}_f + u'_f. \tag{9}$$

The local fluctuating velocities are obtained by multiplying the root-mean square (RMS) fluid fluctuating velocity ($u'_{f,rms} = v'_{f,rms} = w'_{f,rms} = (2k/3)^{0.5}$) by random numbers ($N_u, N_v, N_w$) generated from a Gaussian probability density function of zero mean and unity standard deviation at the start of one eddy-particle interaction. The random numbers are maintained constant during one eddy interaction, while respective RMS values are varied according to the particle position (see MacInnes & Bracco, 1992). Note that the above particle equations of motion may not be valid for very small particles (much smaller than 1 μm when human inhalation rates are considered), because of the absence of random force terms responsible for Brownian motions of particles as well as the absence of Cunningham slip factors. In the present report, the Saffman (1965) lift force is also not considered. See Finlay (2001) for more details on Brownian motions, Saffman lift and Cunningham slip factors.

6. Particle tracking algorithm

In order to assure modeling control and flexibility, a tracking algorithm was developed to calculate the trajectory of particles released numerically in the flow field predicted by CFX-TASCflow. This

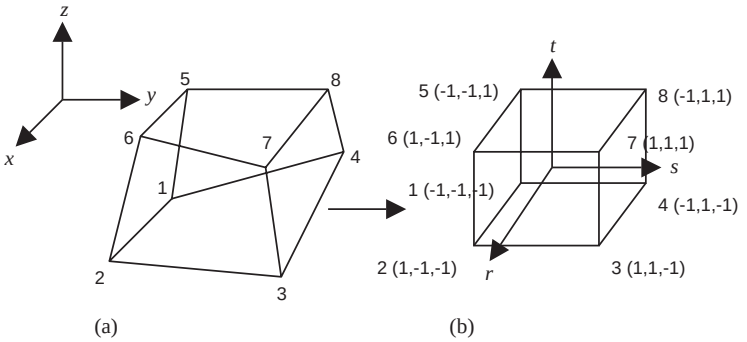

Fig. 4. Transformation of the hexahedric element: (a) in global *xyz* system; (b) in local *rst* system.

algorithm transforms the actual hexahedric elements in the global *xyz* system used by CFX-TASCflow into isoparametric elements in local *rst* system as shown in Fig. 4. A single particle is tracked bysolving the particle equations of motion (4)–(6) (using forth-order Runge–Kutta method) inside the element until the value of r, s or t becomes smaller than -1 or greater than 1, i.e., the particle enters a new element. The connectivity between the elements and between major blocks of the geometry is recognized by the algorithm through pre-stored mappings (manipulated from a CFX-TASCflow post-processed file). Mean velocities, kinetic energy, and dissipation of the flow at the particle position are calculated using trilinear interpolation. Particles are assumed to deposit on and stick to the walls of the idealized geometry when the centroids of the particles reach a distance from the wall equivalent to the radius of the particle. Many particles (1000 for each particle diameter) with various diameters (1.0, 1.5, 2.5, 5, 7.5 and 12.5 μm for 90.0 l/min and 1.7, 4.3, 6.9, 11.3 and 26.0 μm for 30.0 l/min) and density $\rho_p = 912\ \mathrm{kg/m^3}$ are released in the calculated flow domain and particle deposition positions are recorded. Calculations with 10,000 particles have shown negligible differences in total percent deposition, indicating that the number of released particles ($n_p = 1000$) is adequate. Initial particle velocities are set equal to the fluid velocity. The present tracking algorithm was also verified against the tracking module available in the CFX-TASCflow package showing good agreement within approximately 3.0%.

Calculations were distributed on an IBM RS/6000 workstation, Pentium III cluster machines at the Computing and Network Services of the University of Alberta and Alpha cluster machines at the University of Calgary. Each calculation of 1000 particles required up to approximately 50 CPU hours depending on particle diameter, machine and FORTRAN compiler. The calculation time step used in the integration of the particle equation of motion is adaptive and set at each start of an eddy-particle interaction or when the particle enters a new element. The time step is chosen to be the minimum value between $\tau_e/5$ and one fifth of the minimum side length of the local element divided by the particle local velocity, $L_{\min}/(u_p^2 + v_p^2 + w_p^2)^{1/2}$. The Lagrangian time scales, τ_L, are imposed to have a minimum value of 10^{-5} s. This approach circumvents the stiffness problem that occurs near the walls, where eddy lifetimes asymptote to infinitesimal values. The time step should also not exceed the local particle relaxation time, τ_p/α. Up to ten times finer resolution in the time steps and the minimum value of the Lagrangian time scales indicated negligible influence in the final particle deposition results.

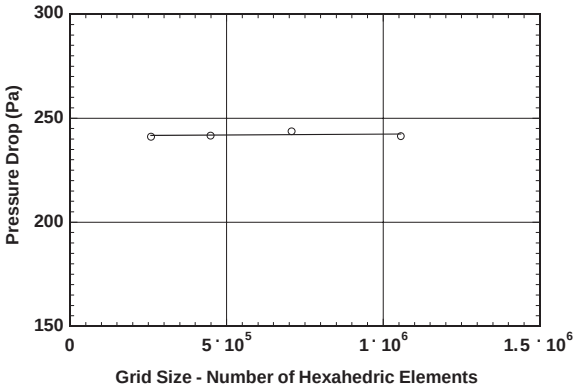

Fig. 5. Grid size effect on pressure drop (inertial parameter, $\rho_p d_p^2 Q = 3078$).

The relation between the natural and the Cartesian coordinates is given as follows:

$$x = \sum_{i=1}^{8} N_i x_i, \quad y = \sum_{i=1}^{8} N_i y_i, \quad z = \sum_{i=1}^{8} N_i z_i, \tag{10}$$

where

$$N_i = \tfrac{1}{8}[1 + (r_i)r][1 + (s_i)s][1 + (t_i)t], \tag{11}$$

for $i = 1, 2, \ldots, 8$ indicating the vertices of the hexahedron and r_i, s_i and t_i assuming accordingly values of -1 or 1 as in Fig. 4. From the actual position of the particle in the Cartesian coordinate (x, y, z), the position of the particle in the natural coordinate (r, s, t) can be determined numerically. Trilinear interpolation of variables (ϕ) like fluid mean velocities, turbulence kinetic energy and dissipation can be determined by

$$\phi(x, y, z) = [N_1 \;\; N_2 \;\; \ldots \;\; N_8] \begin{bmatrix} \phi_1 \\ \phi_2 \\ \ldots \\ \phi_8 \end{bmatrix}, \tag{12}$$

where ϕ_i $(i = 1\text{–}8)$ are nodal values of these variables.

7. Grid convergence test

Several authors (for example, Roache, 1997; Stern, Wilson, Colman, & Peterson, 2001) have pointed out the importance of the assessment of the numerical uncertainty in CFD calculation. In the present report, the grid generation error was tested with four different grid sizes. Total deposition of particles, pressure drop through the mouth and throat geometry and the mean velocities in two sections were chosen as checking parameters. In Fig. 5, pressure drop through the model is shown to be nearly constant when plotted against the grid resolution for $Q = 90.0$ l/min, indicating the

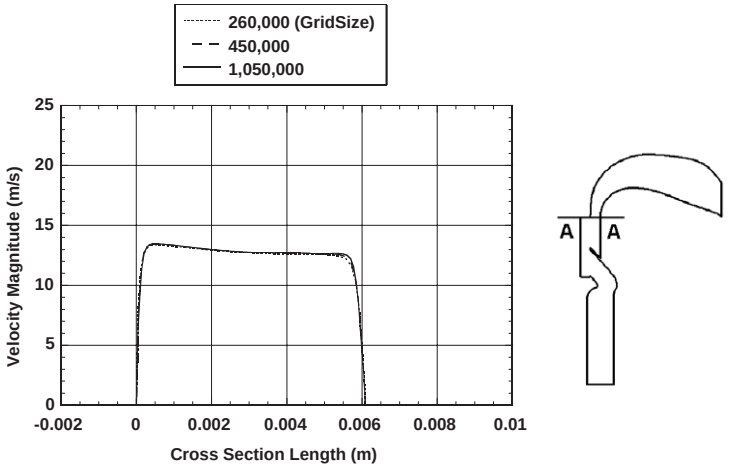

Fig. 6. Grid size effect on mean velocities (Middle section A-A). Inhalation flow rate, $Q = 90.0$ l/min.

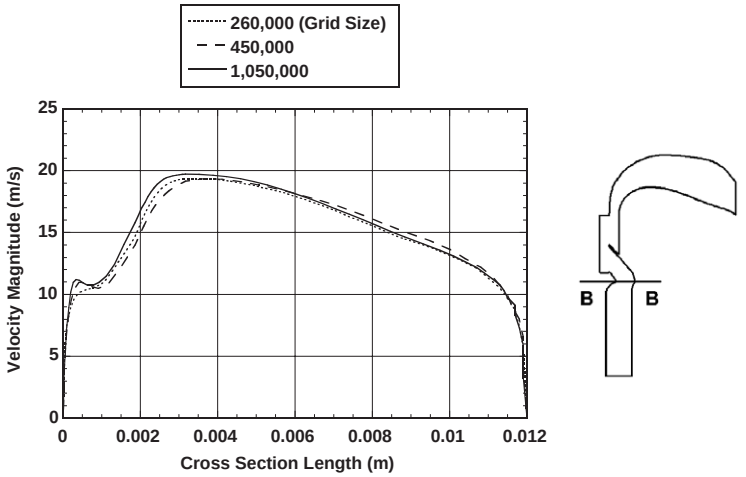

Fig. 7. Grid size effect on mean velocities (Middle section B-B). Inhalation flow rate, $Q = 90.0$ l/min.

adequacy of our grid resolution for the fluid motion. Figs. 6 and 7 show the magnitude of the mean velocity vectors for different grid sizes and constant inhalation flow rate, $Q = 90.0$ l/min, at the middle ending section of the mouth and at the middle section of the glottis (or vocal cords, corresponding to the smallest cross section in the idealized geometry used here), respectively. Except for the region near the walls, there are no major differences in the mean velocities at these sections for different grid sizes, again indicating we have adequately resolved the fluid mechanics. Fig. 8 shows the influence of the grid resolution on the particle deposition results for a low value of inertial parameter, $\rho_p d_p^2 Q = 3078$, with particle diameter, $d_p = 1.5$ μm, and inhalation flow rate of $Q = 90.0$ l/min. In this calculation, "mean flow tracking" (defined in Section 8) was done. Fig. 8

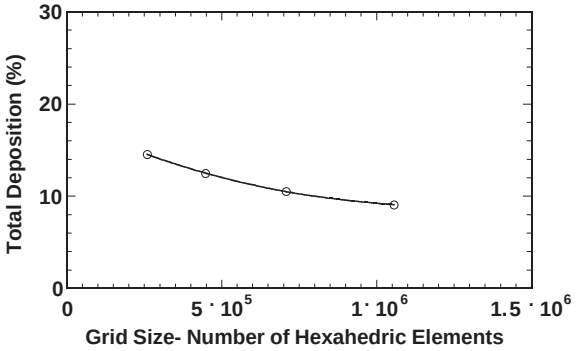

Fig. 8. Grid size effect on particle deposition (inertial parameter, $\rho_p d_p^2 Q = 3078$).

shows that the particle deposition is monotonically converging for the grid size with 1,050,000 hexahedric elements adopted here. Comparing Figs. 6–8, small differences of mean velocities near the wall seem to be affecting particle deposition and a relatively well-refined grid resolution is crucial in the calculation of particle deposition for the present geometry. It must be pointed out that all calculations performed here have enough number of iterations to assure iteration convergence concerning RMS residuals for velocities, mass flow rate and total particle deposition through the idealized mouth–throat geometry.

8. Results of standard EIM calculation of particle deposition

Particle deposition results for an inhalation flow rate of $Q = 90.0$ l/min with the standard k–ω and the standard k–ε models (both with Kato & Launder, 1993, modification) are shown in Fig. 9 in comparison with the experimental fitting curve of Stahlhofen et al. (1989, solid bold line). Dashed lines represent the "turbulent tracking" following Schuen's velocity scales, u_e, and Lagrangian time scales, τ_L. Dotted lines give the results of "mean flow tracking" where particles are made to follow or deviate from the mean flow field according to their inertia only, simply by imposing the local fluctuation velocities to be zero, for example $u'_f = 0$ in Eq. (9). Note that the standard k–ε model has the same number of nodes but uniform grid, with the first nodes from the wall placed at a distance of $y^+ > 10$. Compared to the k–ω model, the standard k–ε model overpredicts deposition for both "turbulent" and "mean flow tracking". It is also clearly seen that the "turbulent tracking" calculation overestimates total deposition over the entire range of inertial parameter, $\rho_p d_p^2 Q$, when compared to the Stahlhofen et al. (1989) curve. Although the standard k–ε model "mean flow" tracking (thin dotted line) seems to agree better with the Stahlhofen's curve (bold line), the standard k–ω model (bold dotted line) is known to have better overall performance for wall and turbulent shear stress distributions, stability, etc. (Menter, 1994) than the standard k–ε model and should be considered more realistic. The k–ω based ASM (Algebraic Stress Model, Speziale & Gatski, 1993) and k–ω SST (Shear Stress Transport, Menter, 1994) were also tested and had similar particle deposition results when compared to the standard k–ω model. Considering the overall superior performance against the standard k–ε model and computational time saving advantages when compared to the

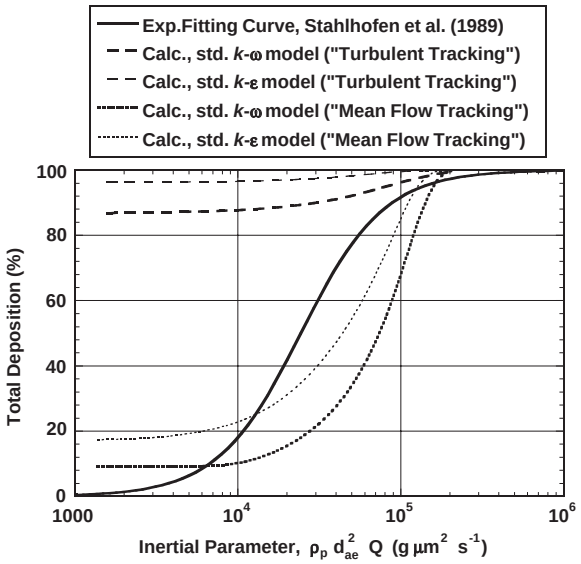

Fig. 9. Total deposition from calculation for different turbulence models in an idealized mouth–throat geometry compared to Stahlhofen et al. (1989) in human subjects. "Turbulent Tracking" indicates the results from the standard eddy interaction model (EIM), while "Mean Flow Tracking" indicates the results obtained with no turbulent particle dispersion, i.e., fluctuating velocities are set to zero in the particle equations. The flow was calculated using an Inhalation flow rate of $Q = 90.0$ l/min.

k–ω based ASM and k–ω SST models, the standard k–ω model (with Kato & Launder, 1993, modification) was adopted for the remainder of this study.

Fig. 10 shows the calculations for inhalation mass flow rates of 90.0 and 30.0 l/min in comparison with the total deposition efficiencies of Stahlhofen et al. (1989, solid bold line). It is clearly seen again that the "turbulent tracking" calculation overestimates total deposition over the entire range of inertial parameter, $\rho_p d_p^2 Q$, at 90.0 l/min and for $\rho_p d_p^2 Q \leqslant 40,000$ at 30.0 l/min. An overall underestimation against Stahlhofen et al. (1989, solid bold line) for $\rho_p d_p^2 Q \geqslant 7000$ and a small overestimation for $\rho_p d_p^2 Q \leqslant 7000$ are obtained for both 90.0 and 30.0 l/min "mean flow tracking" calculations, but in general better agreement with the experimental values is observed than with the "turbulent tracking" calculations. The better agreement of the "mean flow tracking" may be due to the removal of artificially high near wall turbulent diffusivity, i.e., full suppression of this diffusivity gives better results. This suggests that an approach to improve the turbulent tracking would be able to address the excessive near-wall turbulent diffusivity by introducing a correction in the EIM of the "turbulent tracking", as proposed in the following section.

9. Correction of the eddy velocity scales near the wall

Matida, Nishino, and Torii (2000) have shown that the isotropic decomposition of the turbulence kinetic energy ($u'_{f,rms} = v'_{f,rms} = w'_{f,rms} = (2k/3)^{1/2}$) causes an overprediction of particle deposition for small particles (dimensionless relaxation time, $\tau_p^+ < 10$) in a turbulent pipe flow and also that

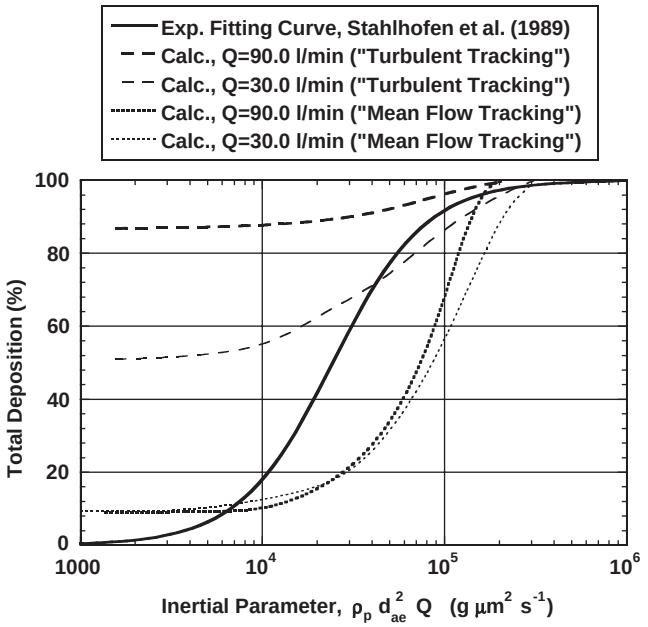

Fig. 10. Total deposition from standard k–ω turbulence model calculation for different inhalation flow rates in an idealized mouth–throat geometry compared to Stahlhofen et al. (1989) in human subjects.

once anisotropy is considered, particle deposition prediction is remarkably improved. To take into account anisotropy and using DNS (direct numerical simulation) channel data results, Wang and James (1999) introduced three functions, f_u, f_v and f_w for the determination of the local fluctuating velocities:

$$u'_{\mathrm{f}} = f_u N_u (2k/3)^{1/2}, \tag{13}$$

$$v'_{\mathrm{f}} = f_v N_v (2k/3)^{1/2}, \tag{14}$$

$$w'_{\mathrm{f}} = f_w N_w (2k/3)^{1/2}, \tag{15}$$

where N_u, N_v and N_w are random numbers generated from a Gaussian probability density function and the functions are expressed as

$$f_u = 1 + 0.285(y^+ + 6)\exp\lfloor -0.455(y^+ + 6)^{0.53} \rfloor, \tag{16}$$

$$f_v = 1 - \exp(-0.02 y^+), \tag{17}$$

$$f_w = \sqrt{(3 - f_u^2 - f_v^2)}, \tag{18}$$

for values of y^+ less than approximately 80. Although, these functions were developed for the channel flow, they are expected to give better values of fluctuations near the wall than those given when isotropy is assumed.

Considering that the fluctuating component normal to the walls plays a major role when particle deposition is concerned and taking into account that the complexity of the present geometry and fluid flow would impose great difficulties in determining the three functions described by Eqs. (16)–(18), a new turbulence kinetic energy for use in the particle tracking calculations is proposed here:

$$k_{\mathrm{dep}} = \frac{3v'^2}{2} = \frac{3}{2}\,[f_v(2k/3)^{0.5}]^2 = f_v^2 k = [1 - \exp(-0.02y^+)]^2 k. \tag{19}$$

This correction uses only the normal function f_v and applies it to all three velocity components. In the eddy-interaction model, this gives

$$\tau_{\mathrm{e}} = 2\tau_{\mathrm{L}} = 2\,\frac{1}{2}\,\frac{(C_\mu)^{3/4}}{(2/3)^{1/2}}\,\frac{k_{\mathrm{dep}}}{\varepsilon} = 0.2\,\frac{k_{\mathrm{dep}}}{\varepsilon}, \tag{20}$$

with τ_{e} maintained constant during one eddy-particle interaction and

$$u_{\mathrm{e}} = f_v(2k/3)^{1/2} = (2k_{\mathrm{dep}}/3)^{1/2} \tag{21}$$

or

$$u'_{\mathrm{f,rms}} = v'_{\mathrm{f,rms}} = w'_{\mathrm{f,rms}} = [1 - \exp(-0.02y^+)](2k/3)^{1/2}. \tag{22}$$

Since the particles used in the present calculation are relatively small, crossing trajectory effects are not relevant and the length scales can be neglected. The turbulence kinetic energy, k, was optimized and corrected up to y^+ approximately equal to 20 ($Q = 90.0$ l/min) and to 1 ($Q = 30.0$ l/min) in the present simulation, in regions which are in the buffer layer and the laminar sublayer near the wall (distant from the turbulent core). The use of Eq. (22) will lead to an underestimation of $u'_{\mathrm{f,rms}}$ and $w'_{\mathrm{f,rms}}$, but this has no great effect when particle deposition from a turbulent flow towards the surrounding walls is concerned.

The new correction was implemented in the "turbulent tracking" and the results are shown in Fig. 11. The thin continuous line and the thin dashed line show the results of the present calculation with the near-wall turbulence correction for 90.0 and 30.0 l/min, respectively. The new results show a substantial improvement over the previous cases and a relatively good agreement with the Stahlhofen et al. (1989) curve, supporting the effectiveness of the correction. There is a small underestimation for approximately $\rho_{\mathrm{p}} d_{\mathrm{p}}^2 Q \geqslant 10,000$ and a small overestimation for $\rho_{\mathrm{p}} d_{\mathrm{p}}^2 Q \leqslant 10,000$, but these are much smaller than in the "turbulent tracking" and the "mean flow tracking" calculations shown in Fig. 10. The remaining discrepancies between the calculation and the experiments can be attributed to limitations of the fluid flow solution, such as turbulence modeling and grid convergence, in addition to the eddy-interaction model used in the present simulation.

The positive effect of the new correction is further supported by a more detailed comparison of the deposition sites within the domain. Fig. 12 shows average local deposition within the geometry from the Grgic et al. (2002) scintigraphy experiment, compared to our results from the standard EIM "turbulent tracking" and our modified EIM "near wall correction" tracking. The data correspond to an inhalation flow rate of Q=90.0 l/min and d_{p}=3.01 μm diameter particles giving an inertial parameter, $\rho_{\mathrm{p}} d_{\mathrm{p}}^2 Q = 13,146.5$. The geometry was divided in three regions as depicted in the figure. Region #1 goes from the mouth opening to the pharynx, region #2 from the pharynx to the vocal cords and region #3 from the vocal cords to the end of the trachea. The "turbulent tracking" calculation (i.e., standard EIM with k–ω) leads to an overprediction in the regions #1 and #3, and a small underprediction in region #2 when compared to the experimental results. The overall agreement of

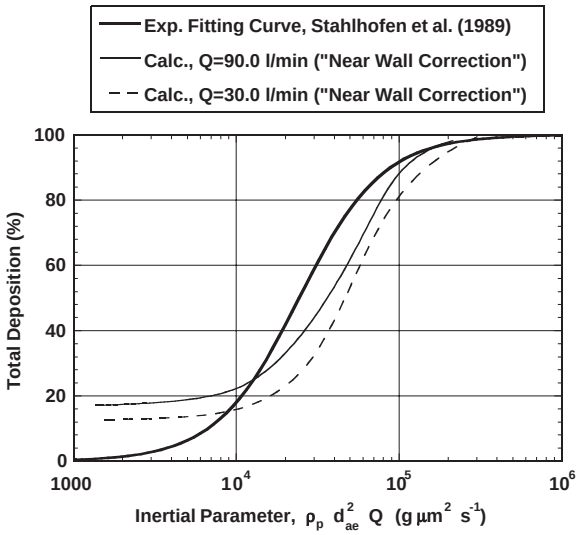

Fig. 11. Total deposition from "near wall correction" on "turbulent tracking" for different inhalation flow rates in an idealized mouth–throat geometry compared to Stahlhofen et al. (1989) in human subjects. The flow was calculated using standard k–ω turbulence model.

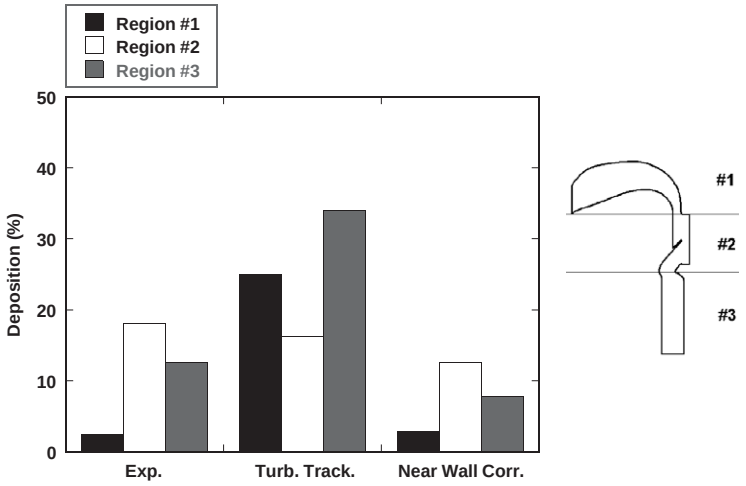

Fig. 12. Localized deposition (inertial parameter, $\rho_p d_p^2 Q = 13,146.5$) in the three regions of the idealized geometry as shown. "Exp." are the experimental data from Grgic et al. (2002), "Turb. Track" are from the standard EIM k–ω calculation and "Near-Wall Corr." are from our modified EIM k–ω calculation.

the "near wall correction" tracking (i.e., modified EIM with k–ω) is clearly superior to the "turbulent tracking". Further improvement in the correction should be focused on the analysis of localized deposition. The examination of total and local depositions has demonstrated that the Lagrangian eddy-particle interaction model itself is capable of predicting particle deposition if adequate correction of the fluid eddy velocity scales (fluctuating part) is applied in the simulation.

10. Conclusions

Our present simulation shows that once adequate near-wall corrections along with a well-refined grid are applied, a relatively simple Reynolds averaged Navier–Stokes (RANS) model for the primary flow with Schuen's eddy interaction model (EIM) for the particulate phase can be used in the prediction of the deposition of particles in an idealized mouth–throat geometry. Near wall corrections of the turbulence kinetic velocity used in the EIM are based on the fact that the fluctuating velocity component normal to the walls plays the major role when particle deposition is concerned. Simulated results of total and localized deposition of particles in an idealized mouth–throat geometry with near-wall corrections in the EIM show relatively good agreement (within approximately 20% of total deposition) with experimental data obtained in separate experiments, improving significantly over results obtained without near-wall corrections.

Acknowledgements

The authors gratefully acknowledge the contributions of W. H. DeHaan and A. F. Heenan, and the financial support of the Natural Science and Engineering Research Council of Canada.

References

Beal, K. S. (1970). Deposition of particles in turbulent flow on channel or pipe walls. *Nuclear Science and Engineering*, *40*, 1–11.

Berlemont, A., Desjonqueres, P., & Gousbet, G. (1990). Particle Lagrangian simulation in turbulent flows. *International Journal of Multiphase Flow*, *16*(1), 19–34.

Burry, D., & Bergeles, G. (1993). Dispersion of particles in anisotropic turbulent flows. *International Journal of Multiphase Flow*, *19*, 651–664.

Chen, M., & McLaughlin, J. B. (1995). A new correlation for the aerosol deposition rate in vertical ducts. *Journal of Colloid and Interface Science*, *169*, 437–455.

DeHaan, W. H., & Finlay, W. H. (2001). In vitro monodisperse aerosol deposition in a mouth and throat with six different inhalation devices. *Journal of Aerosol Medicine*, *14*(3), 361–367.

Elgobashi, S. (1994). On predicting particle-laden turbulent flows. *Applied Scientific Research*, *52*, 309–329.

Finlay, W. H. (2001). *The mechanics of inhaled pharmaceutical aerosols: An introduction*. New York: Academic Press.

Friedlander, S. K., & Johnstone, H. F. (1957). Deposition of suspended particles from turbulent gas streams. *Industrial & Engineering Chemistry*, *49*(7), 1151–1156.

Ganic, E. N., & Mastanaiah, K. M. (1981). Investigation of droplet deposition from a turbulent gas stream. *International Journal of Multiphase Flow*, *7*, 401–422.

Gosman, A. D., & Ioannides, E. (1981). Aspects of computer simulation of liquid-fueled combustors. Paper AIAA-81-0323, *American Institute of Aeronautics and Astronautics (AIAA) 19th Aerospace Science Meeting*, St. Louis, MO.

Graham, D. I., & James, P. W. (1996). Turbulent dispersion of particles using eddy interaction models. *International Journal of Multiphase Flow*, *22*(1), 157–175.

Grgic, B., Finlay, W. H., & Heenan, A. K. (2002). Regional aerosol deposition and flow measurements in an idealized mouth and throat. *Journal of Aerosol Science*, in press.

Hennick, E. A., & Lightstone, M. F. (2000). A comparison of stochastic separated flow models for particle dispersion in turbulent flows. *Energy & Fuels*, *14*, 95–103.

Hinze, J. O. (1975). *Turbulence*. New York: McGraw-Hill.

Kallio, G. A., & Reeks, M. W. (1989). A numerical simulation of particle deposition in turbulent boundary layers. *International Journal of Multiphase Flow*, *15*(3), 433–446.

Kato, M., & Launder, B. E. (1993). The modeling of turbulent flow around stationary and vibrating square cylinders. *9th Symposium on turbulent shear flows*, 10-4-1–10-4-6.

Kim, I., Elgobashi, S., & Sirignano, W. A. (1998). On the equation for spherical-particle motion: effect of Reynolds and acceleration numbers. *Journal of Fluid Mechanics*, *367*, 221–253.

Lee, S. L., & Wiesler, M. A. (1987). Theory on transverse migration of particles in a turbulent two-phase suspension due to turbulent diffusion. *International Journal of Multiphase Flow*, *13*(1), 99–111.

Li, W.-I, Perzl, M., Heyder, J., Langer, R., Brain, J., Englmeier, K.-H., Niven, R. W., & Edwards, D. A. (1996). Aerodynamics and aerosol particle deaggregation phenomena in model oral-pharyngeal cavities. *Journal of Aerosol Science*, *27*(8), 1269–1286.

MacInnes, J. M., & Bracco, F. V. (1992). Stochastic particle dispersion modeling and the tracer-particle limit. *Physics of Fluids A*, *4*(12), 2809–2824.

Matida, E. A., Nishino, K., & Torii, K. (2000). Statistical simulation of particle deposition on the wall from turbulent dispersed pipe flow. *International Journal of Heat and Fluid Flow*, *21*, 389–402.

Maxey, M. R., & Riley, J. J. (1983). Equation of motion for a small rigid sphere in a nonuniform flow. *Physics of Fluids*, *26*(4), 883–889.

Mei, R. (1996). Velocity fidelity of flow tracer particles. *Experiments in Fluids*, *22*, 1–13.

Menter, F. R. (1994). Two-Equation eddy-viscosity turbulence models for engineering Applications. *American Institute of Aeronautics and Astronautics (AIAA) Journal*, *32*(8), 1598–1605.

Rahmatalla, M. F., Zuberbuhler, P. C., Lange, C. F., & Finlay, W. H. (2002). In vitro effect of a holding chamber on the deposition pattern of QVAR (Hydrofluoroalkane-beclomethasone dipropionate). *Journal of Aerosol Medicine*, *15*, 379–385.

Reeks, M. W. (1983). The transport of discrete particle in inhomogeneous turbulence. *Journal of Aerosol Science*, *14*(6), 729–739.

Roache, P. J. (1997). Quantification of uncertainty in computational fluid dynamics. *Annual Review of Fluid Mechanics*, *29*, 123–160.

Saffman, P. G. (1965). The lift on a small sphere in a slow shear flow. *Journal of Fluid Mechanics*, *22*(2), 385–400.

Sarangapani, R., & Wexler, A. (2000). Modeling particle deposition in extrathoracic airways. *Aerosol Science and Technology*, *32*, 72–89.

Sato, Y., & Yamamoto, K. (1987). Lagrangian measurement of fluid-particle motion in an isotropic turbulent field. *Journal of Fluid Mechanics*, *175*, 183–199.

Schuen, J. S., Chen, L. D., & Faeth, G. M. (1983). Evaluation of a stochastic model of particle dispersion in a turbulent round jet. *American Institute of Chemical Engineers (AIChE) Journal*, *29*(1), 167–170.

Speziale, C. G., & Gatski, T. B. (1993). Explicit algebraic stress models for complex turbulent flows. *Journal of Fluid Mechanics*, *254*, 59–78.

Stahlhofen, W., Rudolf, G., & James, A. C. (1989). Intercomparison of experimental regional aerosol deposition data. *Journal of Aerosol Medicine*, *2*, 285–308.

Stapleton, K. W., Guentsch, E., Hoskinson, M. K., & Finlay, W. H. (2000). On the suitability of k–ε turbulence modeling for aerosol deposition in the mouth and throat: a comparison with experiment. *Journal of Aerosol Science*, *31*(6), 739–749.

Stern, F., Wilson, R. V., Coleman, H. W., & Paterson, E. G. (2001). Comprehensive approach to verification and validation of CFD simulations—part 1: Methodology and procedures. *Journal of Fluids Engineering*, *123*, 793–802.

Uijttewaal, W. S. J., & Oliemans, R. V. A. (1996). Particle dispersion and deposition in direct numerical and large eddy simulations of vertical flows. *Physics of Fluids*, *8*(10), 2590–2604.

Wang, Y., & James, P. W. (1999). On the effect of anisotropy on the turbulent dispersion and deposition of small particles. *International Journal of Multiphase Flow*, *25*, 551–558.

Wang, Q., Squires, K. D., Chen, M., & McLaughlin, J. B. (1997). On the role of the lift force in turbulence simulations of particle deposition. *International Journal of Multiphase Flow*, *23*(4), 749–763.

Wang, L.-P., & Stock, D. E. (1992). Stochastic trajectory models for turbulent diffusion: Monte Carlo process versus Markov chains. *Atmosphere Environment*, *26A*, 1599–1607.

Wilcox, D. C. (1988). Reassessment of the scale-determining equation. *American Institute of Aeronautics and Astronautics (AIAA) Journal*, *26*(11), 1299–1310.

Yang, Z. W., & Lee, S. L. (1991). On the droplet deposition and mist supercooling in a turbulent channel flow. *Particle & Particle System Characterization*, *8*, 72–78.

Young, J., & Leeming, A. (1997). A theory of particle deposition in turbulent pipe flow. *Journal of Fluid Mechanics*, *340*, 129–159.

Yu, G., Zhang, Z., & Lessman, R. (1998). Fluid flow and particle diffusion in the human upper respiratory system. *Aerosol Science and Technology*, *28*, 146–158.

Zhou, Q., & Leschziner, M. A. (1991). A time correlated stochastic model for particle dispersion in anisotropic turbulence. *8th Symposium on turbulent shear flows*. Technical University of Munich.